Scattering of Light by One- and Two-Magnon Excitations

P. A. FLEURY
Bell Telephone Laboratories, Murray Hill, New Jersey
AND
R. LOUDON
Essex University, Colchester, England
(Received 11 September 1967)

We present details of the theory of light scattering by one- and two-magnon excitations, and compare predictions of the theory with our experimental results in the tetragonal antiferromagnets MnF_2 and FeF_2. Two mechanisms are considered for first-order (one-magnon) light scattering: one involving a direct magnetic-dipole coupling and the other involving an indirect electric-dipole coupling which proceeds through a spin-orbit interaction. Experimental results on the intensity and polarization selection rules of the first-order scattering show that the spin-orbit mechanism is the important one. On the other hand, second-order (two-magnon) scattering is observed to be even stronger than first-order scattering in these antiferromagnets, implying that the process is not due to the spin-orbit mechanism taken to a higher order in perturbation theory. A theory of second-order scattering based on an excited-state exchange interaction between opposite sublattices is given. When coupled with group-theoretical requirements for the D_{2h}^{12} crystals, the mechanism predicts the intensity, the polarization selection rules, and the magnetic field dependence of the second-order spectrum. Features of the second-order spectra are related quantitatively to magnons at specific points in the Brillouin zone. Analysis of both first- and second-order magnon scattering has thus enabled determination of the complete magnon dispersion relation for FeF_2.

I. INTRODUCTION

THE possibility of light scattering by spin waves or magnons was considered theoretically some years ago by Bass and Kaganov[1] and by Elliott and Loudon.[2] These authors examined photon-magnon interactions based on (1) a direct magnetic-dipole coupling and (2) an indirect electric-dipole coupling via a spin-orbit interaction, respectively. More recently Shen and Bloembergen[3] have investigated further the Elliott-Loudon mechanism. Within the past year the first observation of light scattering by magnons was reported[4] in the antiferromagnet FeF_2. Since then similar observations have been reported in MnF_2 [5] and NiF_2.[6] In addition to the one-magnon scattering process that had been treated theoretically, these experiments demonstrated the existence of a relatively strong two-magnon light scattering. Though at first glance the relative strength for the one- and two-magnon processes (the second order is equal to or stronger than the first order) is difficult to explain, it was suggested[4] that while the one-magnon scattering is indeed due to spin-orbit coupling, the two-magnon scattering proceeds through an altogether different mechanism. This mechanism—excited-state exchange interaction—was outlined and tested[5] for the two-magnon process in antiferromagnetic MnF_2, in which the magnon-dispersion relation had been previously measured by neutron scattering.[7]

It is the purpose of this paper to present in full the details of the theory for both one- and two-magnon light scattering and to compare several predictions of the theory with experimental observation. The predictions of the spin-orbit mechanism are confirmed experimentally for the first-order (one-magnon) scattering. Also developed in Sec. II is theory for the second-order (two-magnon) scattering. Predictions emerge regarding the polarization selection rules (Raman tensor symmetry), the intensity, the line shape, and temperature and magnetic field dependence of the scattered light.

In Sec. III we discuss the experimental techniques employed in obtaining the spectra and their temperature and magnetic field dependence. We also present the experimental results on MnF_2 and FeF_2.

Section IV applies the general theory to MnF_2 and FeF_2 and makes numerical comparisons with experiment for these materials. Since the one-magnon process gives the Brillouin-zone-center magnon frequency and the two-magnon process receives its strongest contributions from zone-edge magnons it is tempting to relate the features of the scattered light spectrum to the magnon dispersion relation. This works quite well for MnF_2, where the full magnon dispersion curve has been measured. We are also able—largely because of the simplicity of the magnetic unit cell for these materials—to infer from the light scattering the complete magnon dispersion curve in FeF_2.

Section V concludes the paper with a brief summary and evaluation of light scattering as a technique for

[1] F. G. Bass and M. I. Kaganov, Zh. Eksperim. i Teor. Fiz. **37**, 1390 (1959) [English transl.: Soviet Phys.—JETP, **10**, 986 (1960)].
[2] R. J. Elliott and R. Loudon, Phys. Letters **3**, 189 (1963).
[3] Y. R. Shen and N. Bloembergen, Phys. Rev. **143**, 372 (1966).
[4] P. A. Fleury, S. P. Porto, L. E. Cheesman, and H. J. Guggenheim, Phys. Rev. Letters **17**, 84 (1966).
[5] P. A. Fleury, S. P. Porto, and R. Loudon, Phys. Rev. Letters **18**, 658 (1967).
[6] P. A. Fleury, Bull. Am. Phys. Soc. **12**, 420 (1967).
[7] A. Okazaki, K. C. Turberfeld, and R. W. Stevenson, Phys. Letters **8**, 9 (1964).

studying magnetic materials in comparison with previously employed techniques.

II. GENERAL THEORY OF LIGHT SCATTERING BY MAGNONS

In this section we cover mainly magnon scattering of light in ferromagnets and antiferromagnets. The theory for these two cases is very similar and the calculations for ferromagnets apply to antiferromagnets with only a little extra complication. The theory to be described applies in a general way to any simple ferromagnet or antiferromagnet. However, the emphasis has been determined by the experimental results available. More detailed calculations which apply particularly to the antiferromagnets MnF_2 and FeF_2 will be presented after the experimental results to facilitate comparison.

We first write down some of the standard results[8] from the theory of magnons in ferro- and antiferromagnets which will be required later.

A. Ferromagnetic Magnons

The magnons are quantized excitations of a spin system from its fully aligned ground state. As with any excitation in a periodic structure, magnons may be characterized by a wave vector $\mathbf{k}$. All distinct magnons are generated by allowing $\mathbf{k}$ to take on N values evenly spaced in the Brillouin zone. Here N is the number of unit cells in the crystal sample, there being one spin in each unit cell of a simple ferromagnet.

The magnetic state of the crystal is then specified by the number $n_\mathbf{k}$ of magnons of wave vector $\mathbf{k}$ excited. In thermal equilibrium $n_\mathbf{k}$ is the Bose-Einstein factor appropriate to the magnon energy $E_\mathbf{k}$. It is convenient to define creation and destruction operators $\alpha_\mathbf{k}^\dagger$ and $\alpha_\mathbf{k}$ for the magnons. In the usual way these operators satisfy

$$\alpha_\mathbf{k}^\dagger \mid n_\mathbf{k}\rangle = (n_\mathbf{k}+1)^{1/2} \mid n_\mathbf{k}+1\rangle,$$

$$\alpha_\mathbf{k} \mid n_\mathbf{k}\rangle = n_\mathbf{k}^{1/2} \mid n_\mathbf{k}-1\rangle, \tag{1}$$

and

$$n_\mathbf{k} = \langle n_\mathbf{k} \mid \alpha_\mathbf{k}^\dagger \alpha_\mathbf{k} \mid n_\mathbf{k}\rangle. \tag{2}$$

We consider an insulating ferromagnetic crystal where the magnetic moments are all carried by the spins of electrons which are localized at lattice sites. Assuming a nearest-neighbor isotropic exchange coupling of strength J and a static external field H_0 in the z direction, the ferromagnetic spin Hamiltonian is

$$H = -2J \sum_{\langle i,j\rangle} \mathbf{S}_i \cdot \mathbf{S}_j - g\beta H_0 \sum_i S_i^z, \tag{3}$$

where demagnetization has been neglected, and the first summation runs over pairs of nearest-neighbor spins counting each pair only once.

In the harmonic approximation the spin operators are related to the magnon operators by the transformations

$$S_i^+ = S_i^x + iS_i^y = (2S/N)^{1/2} \sum_\mathbf{k} \alpha_\mathbf{k} \exp(i\mathbf{k}\cdot\mathbf{r}_i),$$

$$S_i^- = S_i^x - iS_i^y = (2S/N)^{1/2} \sum_\mathbf{k} \alpha_\mathbf{k}^\dagger \exp(-i\mathbf{k}\cdot\mathbf{r}_i),$$

$$S_i^z = S - N^{-1} \sum_{\mathbf{k}',\mathbf{k}} \alpha_\mathbf{k}^\dagger \alpha_{\mathbf{k}'} \exp[i(\mathbf{k}'-\mathbf{k})\cdot\mathbf{r}_i], \tag{4}$$

where $\mathbf{r}_i$ is the position of the spin i and S is the magnitude of the spin vector. These transformations diagonalize the Hamiltonian (3), which apart from a constant term becomes

$$H = \sum_\mathbf{k} E_\mathbf{k} \alpha_\mathbf{k}^\dagger \alpha_\mathbf{k}, \tag{5}$$

where

$$E_\mathbf{k} = \hbar\omega_\mathbf{k} = g\beta[H_E(1-\gamma_\mathbf{k}) + H_0] \tag{6}$$

and

$$\gamma_\mathbf{k} = Z^{-1} \sum_{\langle j\rangle} \exp[i\mathbf{k}\cdot(\mathbf{r}_i - \mathbf{r}_j)], \tag{7}$$

the sum being restricted to the nearest-neighbor spins of S_i, and Z being the number of such neighbors. The exchange field H_E is given by

$$g\beta H_E = 2JZS. \tag{8}$$

B. Antiferromagnetic Magnons

The simplest type of antiferromagnet has the spins ordered on two sublattices labeled i and j; the spins on sublattice $i(j)$ point in the positive (negative) z direction. The largest exchange interaction occurs between nearest-neighbor spins on the oppositely directed sublattices, the exchange integral having its sign opposite to that in a ferromagnet. Upon the inclusion of a z-directed anisotropy field H_A, the Hamiltonian for an antiferromagnet takes the form

$$H = 2J \sum_{\langle i,j\rangle} \mathbf{S}_i \cdot \mathbf{S}_j - g\beta H_A[\sum_i S_i^z - \sum_j S_j^z] - g\beta H_0[\sum_i S_i^z + \sum_j S_j^z]. \tag{9}$$

In the magnetic ground state the z components of the total spins on the two sublattices are equal and opposite. The crystal therefore has zero total spin component, $S^z = 0$. In a simple antiferromagnet, each magnetic unit cell contains two spins, one on each sublattice. There are correspondingly two types of magnon for each of the N-allowed wave vectors $\mathbf{k}$ (N is still the number of unit cells in the crystal sample). That is, there are two branches to the magnon dispersion curve. One magnon branch has associated with it excitations involving a change in the total z component of spin to $S^z = -1$, denoted $\mid \downarrow \mathbf{k}\rangle$, while the other magnon branch involves excitations of $S^z = 1$ which are denoted $\mid \uparrow \mathbf{k}\rangle$. If, as

[8] See, for example, C. Kittell, *Quantum Theory of Solids* (John Wiley & Sons, Inc., New York, 1963); V. Jaccarino, in *Magnetism*, edited by G. Rado and H. Suhl (Academic Press Inc., New York, 1963), Vol. 2A, Chap. 5; D. C. Mattis, *Theory of Magnetism* (Harper and Row, New York, 1965).

in the case of the rutile-structure antiferromagnets, the sublattices (i) and (j) are equivalent, these two magnon branches are degenerate in the absence of external fields. Creation and destruction operators $\alpha_{\downarrow k}^{\dagger}$, $\alpha_{\uparrow k}^{\dagger}$, $\alpha_{\downarrow k}$, and $\alpha_{\uparrow k}$ for the two types of magnon are defined in a way analogous to the ferromagnetic case.

Because both magnetic sublattices participate in both types of magnon, the transformation from spin operators to magnon operators in an antiferromagnet required to diagonalize Eq. (9) takes the more complicated form:

$$S_i^{+}=(2S/N)^{1/2}\sum_k(u_k\alpha_{\downarrow k}+v_k\alpha_{\uparrow -k}^{\dagger})\exp(i\mathbf{k}\cdot\mathbf{r}_i),$$
$$S_i^{-}=(2S/N)^{1/2}\sum_k(u_k\alpha_{\downarrow k}^{\dagger}+v_k\alpha_{\uparrow -k})\exp(-i\mathbf{k}\cdot\mathbf{r}_i),$$
$$S_j^{+}=(2S/N)^{1/2}\sum_k(v_k\alpha_{\downarrow -k}+u_k\alpha_{\uparrow k}^{\dagger})\exp(-i\mathbf{k}\cdot\mathbf{r}_j),$$
$$S_j^{-}=(2S/N)^{1/2}\sum_k(v_k\alpha_{\downarrow -k}^{\dagger}+u_k\alpha_{\uparrow k})\exp(i\mathbf{k}\cdot\mathbf{r}_j). \quad (10)$$

The S^z transformations are obvious generalizations of (4). Each magnon excited changes the z component of the total spin of one sublattice by $\pm u_k^2$ and of the other sublattice by $\mp v_k^2$. The requirement

$$u_k^2-v_k^2=1 \quad (11)$$

ensures that the excitation of a single magnon changes the spin component of the entire crystal by ± 1. The coefficients u_k and v_k are given more explicitly by

$$u_k=\cosh\tfrac{1}{2}\theta_k,$$
$$v_k=\sinh\tfrac{1}{2}\theta_k, \quad (12)$$

where

$$\tanh\theta_k=-\gamma_k/[1+(H_A/H_E)], \quad (13)$$

γ_k and H_E being given by (7) and (8). Note that θ_k, and hence also v_k, are normally negative in the first Brillouin zone. Figure 1 shows the variation of u_k^2 and v_k^2 with $\mathbf{k}$ for MnF_2 in the (100) direction, $\mathbf{k}_{max}$ being the zone-boundary wave vector. Notice that for $\mathbf{k}\ll\mathbf{k}_{max}$, magnons of both branches $|\uparrow\mathbf{k}\rangle$ and $|\downarrow\mathbf{k}\rangle$ perturb both sublattices substantially. However, when $\mathbf{k}$ is close to the zone boundary, v_k^2 is the small and the excitations $|\uparrow\mathbf{k}\rangle$ propagate mainly on the j sublattice while the magnons $|\downarrow\mathbf{k}\rangle$ propagate mainly on the i sublattice. These conclusions hold for any direction of $\mathbf{k}$ in MnF_2 but are not necessarily correct for other crystal structures.

The transformations (10) diagonalize the Hamiltonian (9) which becomes, apart from a constant term,

$$H=\sum_k[E_{\uparrow k}\alpha_{\uparrow k}^{\dagger}\alpha_{\uparrow k}+E_{\downarrow k}\alpha_{\downarrow k}^{\dagger}\alpha_{\downarrow k}], \quad (14)$$

where

$$E_{\downarrow k}=E_k+g\beta H_0,$$
$$E_{\uparrow k}=E_k-g\beta H_0, \quad (15)$$
$$E_k=\hbar\omega_k=g\beta H_E[(1+H_A/H_E)^2-\gamma_k^2]^{1/2}. \quad (16)$$

It is now obvious that the two types of magnon have the same excitation energy in the absence of an external magnetic field.

The theory reviewed above should apply rigorously to insulating crystals where the magnetic ions have ground states of zero orbital angular momentum L, e.g., Mn^{2+}, Fe^{3+}, Eu^{2+}, and Gd^{3+}. However, the theory should also apply well to crystals where the magnetic ion is a transition-metal ion having quenched orbital angular momentum. This is the case for example for Fe^{2+} in FeF_2. We refer to magnetic-ion ground states which are orbitally nondegenerate as $L=0$ ground states, including in this category both genuine S ground states and crystalline-field quenched ground states.

For magnetic ions which do not have $L=0$ ground states, the magnetic excitations are more difficult to treat. This category of crystal includes those where the magnetic-ion ground state is orbitally degenerate, or where the lifting of the ground-state degeneracy by crystal-field effects is smaller than or comparable to the exchange energy. We do not present any detailed theory for light scattering by these more complex excitations, but include in Sec. IV B a brief discussion of the symmetry characteristics of the scattering.

C. First-Order Scattering

Consider an experiment in which the incident radiation has angular frequency ω_1 and the scattered frequency is ω_2. For Stokes scattering the difference $\omega_1-\omega_2$ is equal to the frequency ω_0 of the magnon created. By the usual wave-vector conservation arguments for first-order Raman scattering, the magnon has a wave

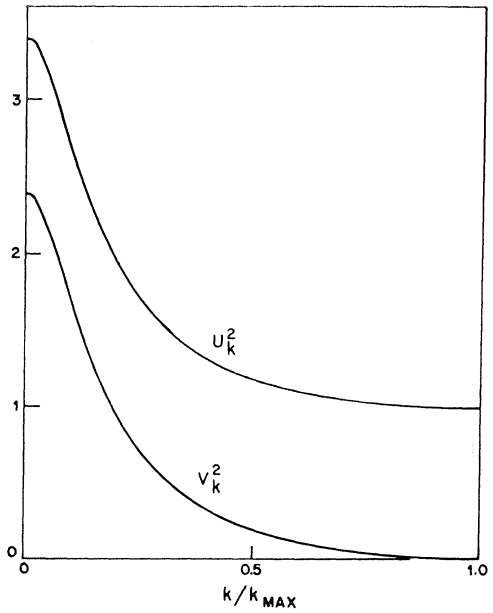

FIG. 1. Variation of u_k^2 and v_k^2 in MnF_2 as functions of k in the (100) direction. The values at the two ends of the k/k_{max} scale are the same for any direction.

vector $\mathbf{k}$ close to the center of the Brillouin zone. Thus from (7) γ_k is unity and for a ferromagnet according to (6)

$$\hbar\omega_0 = g\beta H_0, \tag{17}$$

while for an antiferromagnet, according to (15) and (16),

$$\hbar\omega_0 = g\beta[(2H_E + H_A)H_A]^{1/2} \pm g\beta H_0. \tag{18}$$

For easily obtainable magnetic fields $g\beta H_0$ corresponds to a frequency of order 1–5 cm^{-1}. The frequency shift in a ferromagnet is consequently too small to be easily detected in a conventional Raman spectrograph. On the other hand, $\hbar\omega_0$ for an antiferromagnet even in zero applied field can be quite large. For example, ω_0 is ~ 52 cm^{-1} in FeF_2.[9]

The first proposal for a Raman-scattering experiment using magnon excitation was made by Bass and Kaganov.[1] They considered Raman scattering from a ferromagnet using the direct magnetic-dipole interaction between the spin system and the electromagnetic field. $H_{MD} = -g\beta \sum \mathbf{H}_i \cdot \mathbf{S}_i$, where g, β, and $\mathbf{S}_i$ have their usual meanings and $\mathbf{H}_i$ is the magnetic field of the light wave at site i. The magnetic-dipole Raman-scattering process occurs in the second order of time-dependent perturbation theory using H_{MD} as the perturbation. It depends on the fact evident from (4) that the z component of the magnetic vector of the radiation couples to S_i^z which scatters a magnon, while the x and y components are associated with creation or destruction of a single magnon. Thus a mechanism for the Stokes component of the scattered radiation is obtained using magnon creation for one interaction with the radiation and magnon scattering for the other.

There are two contributions to the perturbation expansion, differing in the time order of the absorption of the ω_1 photon and the emission of the ω_2 photon. The extinction coefficient, defined as the fraction of light scattered per cm of path length per unit solid angle, is found to be

$$h = \frac{(g\beta)^3 M_s \eta_1 \eta_2^3 \omega_1 \omega_2^3 (n_0+1)}{2\hbar^2 c^4} \left| \frac{h_1^+ h_2^z}{\omega_0 - \omega_1} + \frac{h_2^+ h_1^z}{\omega_0 + \omega_2} \right|^2 .$$

In this expression subscripts 1 and 2 refer throughout to quantities associated with the incident and scattered radiation, respectively, $M_s = g\beta NS/V$ is the saturation magnetization, and n_0 is the Bose-Einstein factor for the magnons of frequency ω_0. Apart from the temperature-dependent factor, the above result is identical to that for Raman scattering by a density of N/V paramagnetic spins per unit volume. $h^+ = h^x + ih^y$ and represents a unit vector in the direction of the *magnetic* field of the optical wave.

For scattering of incident light in the optical or infrared regions of the spectrum where $\omega_1 \gg \omega_0$ and $\omega_1 \approx \omega_2$, we obtain the simplified result

$$h = [(g\beta)^3 M_s \eta_1 \eta_2^3 \omega_1^2 (n_0+1)/2\hbar^2 c^4][(h_1^z h_2^z - h_1^x h_2^x)^2 + (h_1^z h_2^y - h_1^y h_2^z)^2].$$

For typical values of the saturation moment and refractive indices, and assuming exciting radiation of wavelength 5000 Å, the order of magnitude of h is

$$h \approx 10^{-13}(n_0+1) \text{ cm}^{-1} \text{ sr}^{-1}. \tag{19}$$

The values of h observed experimentally are much larger than this, and the polarization selection rules observed are not those predicted by the Bass-Kaganov mechanism.[10] So we conclude it can be ignored here.

A more efficient scattering mechanism is provided by the electric-dipole coupling of the radiation to the crystal. Although the electric vector of the radiation does not interact directly with electronic spins, there is an indirect coupling due to the mixing of spin and orbital motions. This mechanism for scattering of light by magnons was pointed out by Elliott and Loudon[11] and is best illustrated by a specific example. Consider a ferromagnetic crystal in which the ground state of the magnetic ion has a spin S and zero orbital angular momentum, $L=0$. We suppose that the ion also has an excited P state with $L=1$ and the same spin S as the ground state. The ground state is split into $2S+1$ components by the exchange field, and the excited state is split into three components by the spin-orbit interaction (we ignore the exchange-field splitting of the excited state). These energy levels are sketched in Fig. 2. The energy eigenfunctions $|J, J^z\rangle$ for the spin-

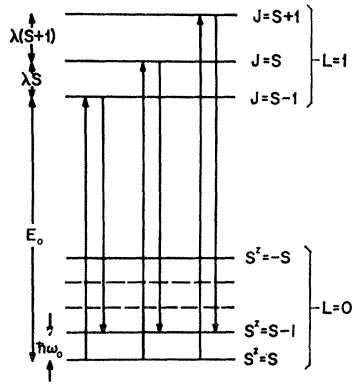

FIG. 2. Energy levels to illustrate the electric-dipole Raman mechanism. E_0 is normally very much larger than λS and $\hbar\omega_0$.

[9] R. C. Ohlmann and M. Tinkham, Phys. Rev. **123**, 425 (1961).

[10] A similar scattering process had been considered earlier for magnetic-dipole couplig to individual atoms in the radio and microwave frequency ranges by J. M. Winter, J. Phys. Radium **19**, 834 (1958) and A. Javan, *ibid.* **19**, 836 (1958).

[11] See Ref. 2. The electric-dipole mechanism for one-magnon scattering has since been discussed by several authors. In addition to Ref. 3, we allude to Y. R. Shen, J. Appl. Phys. **38**, 1490 (1967); and T. Moriya, J. Phys. Soc. Japan **23**, 490 (1967). A useful connection between the Faraday effect and the spin-Raman effect has been noted noted by P. S. Pershan, J. Appl. Phys. **38**, 1482 (1967), among others.

orbit split excited state can be expressed as linear combinations of the unperturbed $|L^z, S^z\rangle$ eigenfunctions in the usual way.[12]

The magnon is a linear combination of the excitations of the individual ions from their $S^z=S$ to their $S^z=S-1$ states. So the first step in computing the magnon Raman transition probability is to calculate the corresponding transition probability for a single magnetic ion. The Raman transition for a single ion can proceed by a pair of allowable electric-dipole transitions via the P excited state. Such pairs are indicated by the vertical arrows in Fig. 2; any of the three spin-orbit split excited states can act as the virtual intermediate state in the double transition. In one of these transitions a quantum of the excited radiation is absorbed and in the other a scattered quantum is emitted. Figure 2 pictures the Stokes scattering only. The energy difference between the $S^z=S$ and $S^z=S-1$ states is denoted $\hbar\omega_0$ in Fig. 2, corresponding to the magnon excitation energy.

The electric-dipole interaction between the radiation and the electrons of the magnetic ions is given by $H_{ED}=-e\sum_i \mathbf{E}_i\cdot\mathbf{r}_i$. The radiative electromagnetic field in a crystal is specified by the vector potential $\mathbf{A}_i$ at the position $\mathbf{r}_i$. In second-quantized notation

$$A_i=c\sum_{\mathbf{k}}(2\pi\hbar/V\omega_{\mathbf{k}}\eta_{\mathbf{k}}^2)^{1/2}\boldsymbol{\varepsilon}_{\mathbf{k}}\exp(i\mathbf{k}\cdot\mathbf{r}_i)(b_{\mathbf{k}}+b_{\mathbf{k}}^{\dagger}),$$

$$E_i=-c^{-1}(d\mathbf{A}_i/dt), \tag{20}$$

where $\eta_{\mathbf{k}}$ is the refractive index at the frequency $\omega_{\mathbf{k}}$ of the radiation, $\mathbf{k}$ and $\boldsymbol{\varepsilon}_{\mathbf{k}}$ are the wave and polarization vectors of the radiation, V is the crystal volume, and $b_{\mathbf{k}}^{\dagger}$ and $b_{\mathbf{k}}$ are photon creation and destruction operators. Taking account of the three possible intermediate states, the total matrix element for the scattering process is

$$M_i=\frac{\pi\hbar e^2(\omega_1\omega_2)^{1/2}\lambda S^{1/2}}{\eta_1\eta_2 V}\left\{\frac{\epsilon_1^z\epsilon_2^+-\epsilon_1^+\epsilon_2^z}{(E_0-\hbar\omega_1)^2}-\frac{\epsilon_1^z\epsilon_2^+-\epsilon_1^+\epsilon_2^z}{(E_0+\hbar\omega_2)^2}\right\}$$
$$\times\langle S,0\,|\,r_i^z\,|\,P,0\rangle\langle P,-1\,|\,r_i^-\,|\,S,0\rangle, \tag{21}$$

where $\hbar\omega_0$ has been neglected in the energy denominators and $\epsilon^+=\epsilon^x+i\epsilon^y$; $r^-=x-iy$. Subscripts 1 and 2 refer to incident and scattered field quantities, respectively. The bra and ket notation is as follows: The capital letter indicates the L value (S or P corresponding to 0 or 1); while the numbers indicate the value of L_z. Already evaluated and incorporated into (21) is the matrix element $\langle P,0\,|\,\lambda L^-S^+\,|\,P,-1\rangle$. Again the spin labels have been omitted from the states since they are obvious. Equation (21) represents the leading term of an expansion in powers of λ/E_0, where λ is the excited-state spin-orbit coupling.

The matrix element M_i connects the $S^z=S$ ground state to the $S^z=S-1$ state. It can therefore be written as an operator linear in S_i^-, using the result

$$S^-\,|\,S,S\rangle=(2S)^{1/2}\,|\,S,S-1\rangle, \tag{22}$$

where the state labels refer to spin values only. The matrix element must now be summed over all the magnetic ions in the crystal. The result is conveniently written in the form of a spin-operator Hamiltonian,

$$H_S^{\text{Stokes}}=\Gamma\sum_i(E_1^zE_2^+-E_1^+E_2^z)S_i^-, \tag{23}$$

where

$$\Gamma=(e^2\lambda/2^{3/2})\langle S,0\,|\,r^z\,|\,P,0\rangle\langle P,-1\,|\,r^-\,|\,S,0\rangle$$
$$\times\{[1/(E_0-\hbar\omega_1)^2]-[1/(E_0+\hbar\omega_2)^2]\}. \tag{24}$$

In these expressions the electric field vectors $\mathbf{E}_1$ and $\mathbf{E}_2$ of the exciting and scattered radiation are to be evaluated at the appropriate ion site i. The matrix elements in (24) do not depend on the particular ion considered, and Γ has accordingly been taken outside the summation in (23).

The final step is to replace the spin operators in (23) by magnon operators. This can be done by means of (4), and again using (20) the result is

$$H_S^{\text{Stokes}}=[(2\pi)^4\hbar(2\omega_1\omega_2SN)^{1/2}/\eta_1\eta_2V^2]$$
$$\times\Gamma(\epsilon_1^z\epsilon_2^+-\epsilon_1^+\epsilon_2^z)\sum_{\mathbf{k}}\alpha_{\mathbf{k}}^{\dagger}\delta(\mathbf{k}_1-\mathbf{k}_2-\mathbf{k}). \tag{25}$$

The scattering is now a first-order process in the effective interaction Hamiltonian H_S^{Stokes} and the extinction coefficient is found by an application of the Golden Rule to be

$$h=[2M_s\eta_2\omega_1\omega_2^3(n_0+1)/g\beta\eta_1c^4]\Gamma^2\,|\,\epsilon_1^z\epsilon_2^+-\epsilon_1^+\epsilon_2^z\,|^2. \tag{26}$$

It is difficult to estimate h numerically because of a lack of knowledge of the matrix elements and energy denominators in the expression for Γ. A range of typical values leads to the rough estimate

$$h\sim(10^{-10}\text{ to }10^{-5})(n_0+1)\text{ cm}^{-1}\text{ sr}^{-1}, \tag{27}$$

assuming optical or near-infrared excitation, much larger than the magnetic-dipole result (19).

The predicted polarization selection rules governing the scattering appear in (26). This form shows for example that exciting light linearly polarized along z gives rise to scattered light which is right-circularly polarized in the xy plane. Note particularly that the scattering is purely *antisymmetric* in the polarizations $\boldsymbol{\varepsilon}_1$ and $\boldsymbol{\varepsilon}_2$ of the incident and scattered light beams. This contrasts with the case of phonons where the scattering is predominantly symmetric[13] in $\boldsymbol{\varepsilon}_1$ and $\boldsymbol{\varepsilon}_2$ and it provides an experimental means for distinguishing magnon scattering from phonon scattering. For example, the magnon Raman scattering vanishes when $\boldsymbol{\varepsilon}_1$ and $\boldsymbol{\varepsilon}_2$ are parallel, regardless of the directions of the incident and scattered wave vectors.

[12] E. U. Condon and G. H. Shortley, *Theory of Atomic Spectra* (Cambridge University Press, Cambridge, England, 1953).

[13] R. Loudon, Proc. Roy. Soc. (London) **A275**, 218 (1963).

The simple antisymmetric form of H_S^{Stokes} for $L=0$ ground states results essentially from the fact that the excitation of a magnon in this case does not involve any change in the orbital states of the magnetic ions; i.e., the magnon is very weakly coupled to the orbital motion. There is a strong analogy here to the Raman scattering from phonons where the purely symmetric form of the scattering results[13] from the fact that, although the coupling of the light waves to the phonons takes place via the intermediary of the electrons, the electronic excitations are entirely virtual, the final electronic state being identical to the initial electronic state. It is well known that for Raman scattering in which an ion is excited to a different final orbital state, the scattering is neither purely symmetric nor purely antisymmetric.

The results analogous to (23) and (24) for the anti-Stokes scattering can be derived straightforwardly and lead to a spin Hamiltonian

$$H_S^{\text{anti-Stokes}}=-\Gamma'\sum_i (E_1^z E_2^- - E_1^- E_2^z) S_i^+, \quad (28)$$

where Γ' is the same as Γ given by (24) except that the energy denominators are reduced by an amount $\hbar\omega_0$. The difference between Γ and Γ' is small, except under resonance conditions where $\hbar\omega_1$ is close to E_0. Setting $\Gamma'=\Gamma$, (23) and (28) combine to give a total spin Hamiltonian which simplifies to

$$H_S=-2i\Gamma\sum_i [(E_1^y E_2^z - E_1^z E_2^y) S_i^x + (E_1^z E_2^x - E_1^x E_2^z) S_i^y]. \quad (29)$$

Notice that this expression is invariant under time-reversal, since this operation reverses the signs of both i and $\mathbf{S}$.

The results derived so far have been based on the energy-level scheme of Fig. 2. A more realistic calculation for a magnetic ion having an S ground state ($L=0$) and several excited $\mathbf{P}$ states leads to identical results, except that a sum over all the P excited states must be taken in the expression (24) for Γ. A further refinement would take into account crystal-field splittings of the excited states.

When the lowest P excited state energy is very much greater than $\hbar\omega_1$ and $\hbar\omega_2$, the square bracket in (21) is approximately $2\hbar(\omega_1+\omega_2)/E_0^3$. This is a small quantity and the largest contribution to Γ in this case may arise not from simple $S\rightarrow P$ virtual excitations but from some more sophisticated type of electric-dipole transition, for example, involving charge transfer or forced electric-dipole vibronic transitions. The formal expression for Γ would be correspondingly modified, but the symmetry of the scattering represented by the spin-Hamiltonian (29) remains valid for an $L=0$ ground state. The symmetry also remains valid for a ground state having quenched orbital angular momentum.

We have treated Raman scattering from a ferromagnet in considerable detail despite the absence of experimental observations in ferromagnets. The reason is that all the results are very easily generalized to the experimentally more interesting antiferromagnetic case.

The total spin Hamiltonian for Raman scattering from a simple antiferromagnet constructed from the magnetic ions of Fig. 2 is

$$H_S=-2i\Gamma\sum_{i,j}[(E_1^x E_2^z - E_1^z E_2^x)(S_i^x+S_j^x) + (E_1^z E_2^y - E_1^y E_2^z)(S_i^y+S_j^y)], \quad (30)$$

where Γ is given by (24) and the $i(j)$ summation runs only over the components of $\mathbf{S}_i(\mathbf{S}_j)$. The Stokes-scattering extinction coefficient is found to be

$$h=[2M_s\eta_2\omega_1\omega_2^3(n_0+1)(u_0+v_0)^2\Gamma^2/g\beta\eta_1 c^4] \times|\,\epsilon_1^z\epsilon_2^+ - \epsilon_1^+\epsilon_2^z\,|^2 \quad (31)$$

for the $\downarrow$ magnon. The result for the $\uparrow$ magnon is the same except that the polarization factor is changed to

$$|\,\epsilon_1^z\epsilon_2^- - \epsilon_1^-\epsilon_2^z\,|^2.$$

Thus for incident light linearly polarized along z the two-magnon branches produce scattered light of opposite circular polarizations in the xy plane.

The discussion following (29) applies to the antiferromagnetic case with a few obvious changes in detail. The main difference from the ferromagnetic case is the appearance in the numerator of (31) of the additional factor $(u_0+v_0)^2$. Expressions for u_0 and v_0 are obtained by setting $\mathbf{k}=0$, $\gamma_k=1$ in (12) and (13). In zero applied magnetic field the result is

$$u_0=\{[g\beta(H_E+H_A)+\hbar\omega_0]/2\hbar\omega_0\}^{1/2}, \quad (32)$$

$$v_0=-\{[g\beta(H_E+H_A)-\hbar\omega_0]/2\hbar\omega_0\}^{1/2}, \quad (33)$$

where

$$\hbar\omega_0=g\beta[(2H_E+H_A)H_A]^{1/2}. \quad (34)$$

It is seen that $(u_0+v_0)^2$ has a maximum value of unity when H_A is much larger than H_E. However it is more common for H_E to be larger than H_A, in which case $(u_0+v_0)^2$ is less than unity. When H_E is much larger than H_A,

$$(u_0+v_0)^2\approx(H_A/2H_E)^{1/2}. \quad (35)$$

Thus as H_A is reduced to zero, both ω_0 and h approach zero as $H_A^{1/2}$ and antiferromagnets with smaller $\mathbf{k}=0$ magnon frequencies tend to be less efficient Raman scatterers. In FeF_2, where ω_0 is 52 cm^{-1}, $(u_0+v_0)^2$ is about 0.4, while in MnF_2[7], where ω_0 is about 8.7 cm^{-1}, $(u_0+v_0)^2$ is about 0.08.

Ferrimagnets have "optical" magnon branches which may be active in first-order scattering. The theory of such scattering requires only a simple extension of the

above work on scattering by ferromagnets and antiferromagnets. Elliott and Loudon[2] have discussed the selection rules which determine how many of the magnon branches in a complicated ferrimagnet are active in first-order Raman scattering.

D. Second-Order Scattering

The second-order Raman effect involves the creation or destruction of a pair of magnons. For the Stokes component of the scattered light the difference in frequency $\omega_1-\omega_2$ is equal to the sum of the frequencies $\omega_{\mathbf{k}}+\omega_{\mathbf{k}'}$ of the two magnons created. Since the wave vectors of the light waves are very small compared with the Brillouin-zone (BZ) edge value of $\mathbf{k}_m$, $\mathbf{k}$ and $\mathbf{k}'$ must be very nearly equal and opposite, i.e., $\mathbf{k}\approx -\mathbf{k}'$. For a ferromagnet having one magnetic ion in the unit cell, $\omega_{-\mathbf{k}}$ is equal to $\omega_{\mathbf{k}}$, and the frequency requirement is

$$\omega_1=\omega_2+2\omega_{\mathbf{k}}. \tag{36}$$

Since $\omega_{\mathbf{k}}$ ranges over a band of values, the second-order Raman radiation is distributed over a band of frequencies.

The distribution of scattered intensity as a function of the frequency ω_2 is largely determined by the number of magnons whose frequency satisfies (36), i.e., the magnon density of states which we denote $\rho(\omega)$.

$$\rho(\omega)=\sum_{\mathbf{k}}^{\mathrm{BZ}}\delta(\omega-\omega_{\mathbf{k}}), \tag{37}$$

where $\mathbf{k}$ runs over all wave vectors in the Brillouin zone. The intensity of the second-order scattering at frequency ω_2 reflects the value of the density of states ρ at the frequency $(\omega_1-\omega_2)/2$. However, the relationship is not generally one of strict proportionality but involves a $\mathbf{k}$-dependent weighting function due to the nature of the coupling. This is illustrated in detail below.

The first-order spin-orbit scattering mechanism discussed in the previous subsection gives rise to a second-order scattering when the calculation is extended to a higher order. The analysis is readily generalized to second-order by modifying Fig. 2 so that the downward pointing arrows end on the $S^z=S-2$ ground-state level (this only works for $S>\frac{1}{2}$). The matrix element for the process can be written as a spin Hamiltonian proportional to $(S_i^-)^2$, and analogous to magnon operators now leads to an expression for the second-order spectrum. However, the second-order coupling constant is smaller than the first-order coupling constant Γ of (24) by a factor of magnitude λ/E_0. Since the factor is squared in expressions for the scattered intensity, the second-order result is normally several orders of magnitude smaller than the first-order result. We note that the second-order spin Hamiltonian for this process would be bilinear in the transverse components of $\mathbf{E}_1$ and $\mathbf{E}_2$.

The same conclusions about the smallness of these two-magnon scattering intensities hold for antiferromagnets. However, one of the most striking features of the original observation[4] of the second-order magnetic Raman spectrum of FeF_2 is the fact that the second-order spectrum is *stronger* than the first-order spectrum. The same is true of MnF_2 and NiF_2. This "anomaly" can be accounted for by a second-order scattering mechanism which is unrelated to the above-discussed process, and is referred to as the exchange-scattering mechanism.[5] As we shall see below, the mechanism applies only to antiferromagnets and is inoperative for ferromagnets where the second-order spectrum is expected to be much weaker than the first-order spectrum.

Let us discuss first the nature of the two-magnon state which is excited as a result of the second-order Stokes scattering in an antiferromagnet. Since there are two magnons having any given wave vector $\mathbf{k}$ and two having wave vector $-\mathbf{k}$, it is possible to form four types of zero-wave-vector two-magnon states as follows:

	S^z	Parity
$\lvert 2,+\rangle=\lvert\uparrow\mathbf{k},\uparrow-\mathbf{k}\rangle$	2	+
$\lvert 0,+\rangle=\lvert\uparrow\mathbf{k},\downarrow-\mathbf{k}\rangle+\lvert\downarrow\mathbf{k},\uparrow-\mathbf{k}\rangle$	0	+
$\lvert 0,-\rangle=\lvert\uparrow\mathbf{k},\downarrow-\mathbf{k}\rangle-\lvert\downarrow\mathbf{k},\uparrow-\mathbf{k}\rangle$	0	−
$\lvert -2,+\rangle=\lvert\downarrow\mathbf{k},\downarrow-\mathbf{k}\rangle$	−2	+.

(38)

Note that the first three states listed in (38) have no analog for a simple ferromagnet having only one magnon branch. In determining the parity it has been assumed that each magnetic ion is a center-of-inversion symmetry I. This is true for MnF_2, FeF_2 and many other common antiferromagnets. The inversion properties of the magnons determined from (10) are

$$\begin{aligned} I\lvert\uparrow\mathbf{k}\rangle&=\lvert\uparrow-\mathbf{k}\rangle,\\ I\lvert\downarrow\mathbf{k}\rangle&=\lvert\downarrow-\mathbf{k}\rangle, \end{aligned} \tag{39}$$

where the invariance of spin vectors under inversion has been used. The parities quoted in (38) now follow.

It is well known that only positive-parity states can be active in Raman scattering. The two-magnon state $\lvert 0,-\rangle$ is thus ruled out for the Raman effect, but it can give rise to a direct electric-dipole absorption process which has been recently observed.[14,15] In an applied magnetic field, (15) shows that $\lvert 0,+\rangle$ and $\lvert 0,-\rangle$ do not shift in first order, whereas the energies of $\lvert 2,+\rangle$ and $\lvert -2,+\rangle$ exhibit linear shifts appropriate

[14] J. W. Halley and I. Silvera, Phys. Rev. Letters **15**, 654 (1965).
[15] S. J. Allen, R. Loudon, and P. L. Richards, Phys. Rev. Letters **16**, 463 (1966).

to $S^z=\pm 2$ states. Thus the three positive-parity two-magnon states can be distinguished experimentally by application of a magnetic field.

Since only $\frac{1}{8}$ of the volume of the Brillouin zone lies within one-half the zone-boundary radius of the origin, the majority of the magnons available for second-order Raman scattering lie in the outer part of the zone. As discussed after (13), such magnons propagate mainly on one or the other of the magnetic sublattices. Thus the two-magnon states $|2,+\rangle$ and $|-2,+\rangle$ each predominantly involve excitation of only one of the sublattices; they would be produced for example by terms $(S_j^+)^2$ and $(S_i^-)^2$, respectively, in the spin Hamiltonian for second-order electric-dipole scattering from an antiferromagnet. On the other hand, the states $|0,+\rangle$ and $|0,-\rangle$ involve a simultaneous excitation of one magnon on each of the sublattices and require intersublattice coupling terms in $S_i^-S_j^+$ for their production. We shall see below that $|0,+\rangle$ is the important state for the second-order Raman observations made to date.

The type of spin operator required to excite the state $|0,+\rangle$ is

$$S_i^-S_j^+ + \text{c.c.} = 2(S_i^xS_j^x + S_i^yS_j^y). \tag{40}$$

Thus any coupling of a pair of light waves to an exchangelike interaction between a pair of spins on opposite sublattices may be effective in producing a second-order Raman effect from the $|0,+\rangle$ state. There are basically two ways in which an exchange interaction can be coupled to a pair of light waves, either via the phonons or via electronic excitations.

The phonon coupling can be envisaged as a two-stage process with a virtual intermediate state: (1) the exciting radiation undergoes ordinary first-order Raman scattering with production of a virtual phonon, and (2) the phonon modulates the exchange integral J in the ordinary exchange interaction and decays into two real magnons via the term $(\partial J/\partial j)\Delta u S_i^-S_j^+$, where u is the vibrational normal coordinate and Δu is the change in u produced by creation or destruction of a single phonon. The effect of this mechanism is difficult to estimate numerically due to lack of knowledge of the quantities $\partial J/\partial u$. It does not appear to be the dominant mechanism in the measurements so far made, as will be discussed below.

The coupling via electronic excitations (the exchange scattering mechanism) is closely related to a mechanism proposed by Tanabe, Moriya, and Sugano[16] to account for the electric-dipole adsorption by the state $|0,-\rangle$ in antiferromagnets. The formal expression for the matrix element is the same as theirs except that an extra stage appears because *two* light waves are required in the Raman effect. Consider two representative ions i and j, one on each sublattice, and suppose that in the ground-state ion i has an electron $\mathbf{r}_1$ with $s^z=\frac{1}{2}$ accommodated in an orbital φ_i, while ion j has an electron $\mathbf{r}_2$ with $s^z=-\frac{1}{2}$ in an orbital φ_j. The interactions of the electrons with the fields and with each other are given by the Hamiltonian

$$H=-e(\mathbf{E}_1+\mathbf{E}_2)\cdot(\mathbf{r}_1+\mathbf{r}_2)+e^2/r_{12}, \tag{41}$$

where $r_{12}=|\mathbf{r}_1-\mathbf{r}_2|$. A representative matrix element for the Raman process accompanied by simultaneous changes in the spin components of ions i and j is

$$M_{ij}=\sum_{\mu,\nu}\frac{\langle\varphi_{i\downarrow}\varphi_{j\uparrow}\,|\,e\mathbf{E}_2\cdot\mathbf{r}_1\,|\,\varphi_{i\downarrow}\varphi_{\nu\uparrow}\rangle\langle\varphi_{i\downarrow}\varphi_{\nu\uparrow}\,|\,e^2/r_{12}\,|\,\varphi_{j\downarrow}\varphi_{\mu\uparrow}\rangle\langle\varphi_{j\downarrow}\varphi_{\mu\uparrow}\,|\,e\mathbf{E}_1\cdot\mathbf{r}_1\,|\,\varphi_{j\downarrow}\varphi_{i\uparrow}\rangle}{(E_\nu+\hbar\omega_k-\hbar\omega_1)(E_\mu-\hbar\omega_1)}. \tag{42}$$

Here φ_μ and φ_ν are any orbitals of ions i and j. In order for the electric-dipole matrix elements to be nonvanishing, the parities of the states which they connect must be opposite. However, there are no strict parity restrictions for the exchange matrix element.

Carrying out a sum over the electrons on ions i and j in (42) and writing

$$V_{ij}{}^{\nu,\mu}=\langle\varphi_{i\downarrow}\varphi_{\nu\uparrow}\,|\,e^2/r_{12}\,|\,\varphi_{j\downarrow}\varphi_{\mu\uparrow}\rangle, \tag{43}$$

the matrix element can be written as an operator:

$$M_{ij}=\left\{\sum_{\mu,\nu}\frac{\langle\varphi_{j\uparrow}\,|\,e\mathbf{E}_2\cdot\mathbf{r}_1\,|\,\varphi_{\nu\uparrow}\rangle V_{ij}{}^{\nu\mu}\langle\varphi_{\mu\uparrow}\,|\,e\mathbf{E}_1\cdot\mathbf{r}_1\,|\,\varphi_{i\uparrow}\rangle}{(E_\nu+\hbar\omega_k-\hbar\omega_1)(E_\mu-\hbar\omega_1)}\right\}S_i^-S_j^+. \tag{44}$$

In addition to the matrix element written out explicitly in (42) and (44) there are many similar matrix elements which connect the initial state $|\varphi_{j\downarrow}\varphi_{i\uparrow}\rangle$ to the final state $|\varphi_{i\downarrow}\varphi_{j\uparrow}\rangle$. These similar matrix elements involve a different ordering of the operators taken from (41) or have $\mathbf{r}_1$ replaced by $\mathbf{r}_2$. It is a standard exercise in third-order perturbation theory to collect all possible terms and we do not write out the complete result in detail.

[16] Y. Tanabe, T. Moriya, and S. Sugano, Phys. Rev. Letters 15, 1023 (1965).

The general expression takes on a simple form when only a single odd-parity excited state φ_0 having energy E_0 is important in the matrix elements. We assume further that E_0 is much larger than $\hbar\omega_1$ and $\hbar\omega_2$ as is experimentally the case for MnF_2 and FeF_2. The total matrix element M_{ij} in this case reduces to

$$M_{ij}\approx\{8e^2\langle\varphi_j \mid \mathbf{E}_2\cdot\mathbf{r}_1 \mid \varphi_0\rangle\bar{V}_{ij}\langle\varphi_0 \mid \mathbf{E}_1\cdot\mathbf{r}_1 \mid \varphi_i\rangle/E_0^2\}S_i^-S_j^+, \tag{45}$$

where $\bar{V}_{ij}$ is some average of the various exchange matrix elements between ions i and j which appear in the general expression.

There is no inherent restriction in (44) on the Cartesian components of $\mathbf{E}_1$ and $\mathbf{E}_2$ which can contribute to the second-order scattering. This contrasts with the scattering via the electric-dipole spin-orbit mechanism discussed above, where only the x and y components of $\mathbf{E}_1$ and $\mathbf{E}_2$ appear. However, for a particular crystal lattice and a given choice of the ions i and j, there will be symmetry restrictions on the allowed components of $\mathbf{E}_1$ and $\mathbf{E}_2$. This will be illustrated presently.

The matrix element M_{ij} and its complex conjugate must now be summed over all pairs of ions i and j on the opposite sublattices. Since an exchange coupling of the ions is involved, M_{ij} can be expected to fall off rapidly with increasing separation of the ions. The appearance of a sum over pairs of ions leads to a dependence of the expressions for the second-order Raman spectrum on the geometrical details of the lattice. These details and others of the theory for the special case of the MnF_2-type lattice will be presented in an analysis of the experimental results, which we discuss in the next section.

Finally, we emphasize that the exchange-scattering mechanism discussed here (being proportional to $S_i^-S_j^+$) produces magnons in pairs and hence there is no exchange-scattering mechanism for one-magnon scattering. Therefore, there exists no *a priori* reason for the second-order light scattering by magnons to be smaller than first-order scattering since the two mechanisms are unrelated. We note also that the exchange mechanism is inoperative for ferromagnets where there is no two-magnon state corresponding to $\mid 0, +\rangle$.

III. EXPERIMENTAL TECHNIQUES AND RESULTS

The experiments discussed here utilized an argon ion laser as the light source. Powers of 50–100 mW of linearly polarized light at either 4880 or 5145 Å were employed. Light scattered by 90° was focused onto the slit of a Spex double monochrometer and analyzed. The scattered light was then detected by an S-11 photomultiplier and the photocurrent dc-amplified and recorded. No pulse-height discrimination, synchronous detection, or photon-counting techniques were necessary in these experiments. The geometry of the incident light, single-crystal sample, and scattered light for a typical experiment is indicated in Fig. 3. By proper positioning of the quartz plate (which rotates by 90° the polarization of light passing through it), the sample, and the polarizer one may examine the Raman tensor element α_{ij} of his choice. [See Eq. (48) below.]

Temperature control of the sample is achieved by a scheme shown in Fig. 4, which employs cold flowing He gas.[17] A range of 6 to 80°K could be conveniently covered with this method. Measurements discussed below using a magnetic field required a different geometry. We used a superconducting solenoid capable of 52-kOe maximum field, with the sample position as indicated in Fig. 5. Temperature variation was not attempted in this configuration. The sample instead remained at a fixed, relatively low temperature (20–30°K) determined by its thermal contact to the liquid He bath of the solenoid and by the radiation heat leaks in the system, including power absorbed from the laser beam. However, the magnetic field geometry did not hamper our ability to explore the polarization selection rules governing the scattering.

The rutile antiferromagnets MnF_2 and FeF_2 become magnetically ordered at 67.7 and 78.5°K, respectively.[7,9] Neutron scattering[7] and infrared absorption[18] experiments indicate that at 0°K the zone-center magnon frequency in MnF_2 is 8.7 cm^{-1} while the zone-edge magnon frequencies are 50 and 55 cm^{-1} at the X and Z points, respectively. In FeF_2, infrared experiments[9,14] indicate 52.7 and $\sim$77 cm^{-1} for the zone-center and zone-edge frequencies, respectively. The Raman-active phonons[19] in MnF_2 have been found to be: $B_{1g}=61$ cm^{-1}; $E_g=247$ cm^{-1}; $A_{1g}=341$ cm^{-1}; and $B_{2g}=476$ cm^{-1} at room temperature. The corresponding phonon frequencies[17] in FeF_2 are 73, 257, 340, and 496 cm^{-1}. As the temperature was lowered below the Néel temperature, additional peaks in the scattered light emerged, as indicated by the early data displayed in Fig. 6 for the

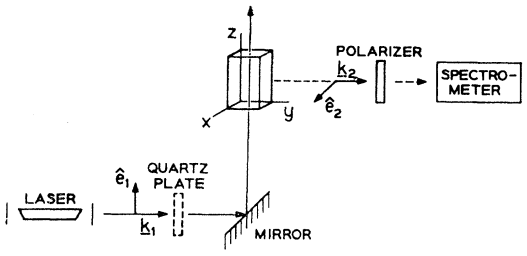

FIG. 3. Schematic of experimental geometry. The vertical direction in the lab is labeled "Z" here, and all directions are with respect to the crystal axes. Light emerges from the laser linearly polarized in the Z direction. The polarization incident upon the sample is determined by inserting or omitting the quartz plate.

[17] M. B. Graifman (private communication).
[18] F. M. Johnson and A. H. Nethercot, Phys. Rev. **114**, 705 (1959).
[19] S. P. S. Porto, P. A. Fleury, and T. C. Damen, Phys. Rev. **154**, 522 (1967).

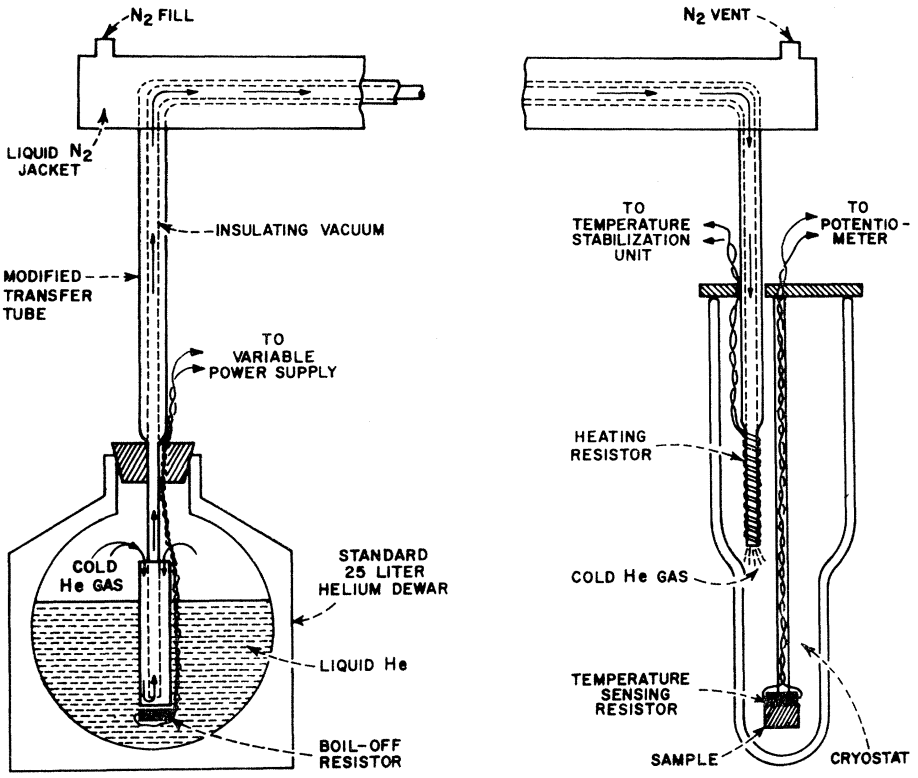

FIG. 4. Temperature control apparatus utilizing flowing He gas. The sample temperature is sensed by a resistor and compared to the desired value. Deviations below and above the desired temperature are corrected by the heating resistor and by increasing the current in the boil-off resistor, respectively.

α_{zx} of FeF_2. The signal to noise has since been improved allowing a higher resolution study of these two lines. (See Fig. 7.) The 52-cm^{-1} line was identified as arising from one-magnon scattering by (1) its polarization: α_{xz}, α_{zx}, α_{yz}, α_{zy} are the only nonzero Raman tensor elements; (2) the temperature dependence of its frequency: It varies as the modified Brillouin function $B_{J=2}$ as does the antiferromagnetic resonance frequency; and (3) it broadens and disappears as T approaches T_N from below. At the lower temperatures (as shown in Fig. 7) the width of the one-magnon line was too small to be measured by our slit settings.

We confirmed that the one-magnon Raman tensor is indeed *antisymmetric* as predicted in (31) by the following techniques. To avoid errors due to birefringence, the incident light was directed so that $\mathbf{k}_1=(-\hat{\imath}k_1/\sqrt{2})+(\hat{k}k_1/\sqrt{2})$; and $\mathbf{E}_1=-(\hat{\imath}/\sqrt{2})E_1-(\hat{k}/\sqrt{2})E_1$, where $\hat{\imath},\hat{\jmath}$, and $\hat{k}$ are unit vectors along the sample's x, y, and z axes, and $\mathbf{k}_1$ and $\mathbf{E}_1$ are the wave vector and electric field of the incident light. The scattered light was observed such that $\mathbf{k}_2=\hat{\imath}(k_2/\sqrt{2})+\hat{k}(k_2/\sqrt{2})$ and $\mathbf{E}_2=-\hat{\imath}(E_2/\sqrt{2})\cos\theta'+\hat{\jmath}E_2\sin\theta'+\hat{k}(E_2/\sqrt{2})\cos\theta'$, where θ' is the setting of the polarizer placed in front of the spectrometer slits. For a symmetric scattering tensor the observed intensity should vary as $\frac{1}{2}(E_1^2E_2^2)\sin^2\theta'$ while an antisymmetric scattering tensor produces

$$\tfrac{1}{2}(E_1^2E_2^2)(1+\cos^2\theta').$$

By measuring the θ' variation for various lines of the FeF_2 spectrum we conclude that: The E_{1g} phonon and the two-magnon peak (154 cm^{-1}) have symmetric Raman tensors; the one-magnon line has an antisymmetric Raman tensor. The same is expected for MnF_2.

The peak at 154 cm^{-1} in FeF_2 was identified as scattering from pairs of zone-edge magnons.[4] This identification was based upon the similarity with the two-magnon absorption peak of Halley and Silvera[14] and the fact that the peak disappears for $T>T_N$. The integrated intensity of the two-magnon scattering in FeF_2 is 2–3 times larger than the one-magnon scattering. Both the $\alpha_{xz}=\alpha_{zx}$ and $\alpha_{xy}=\alpha_{yx}$ are appreciable for the two-magnon peak, but α_{xx}, α_{yy}, α_{zz} are all unobservably small. The α_{xz} and α_{xy} peaks are nearly identical in position and shape for FeF_2, in contrast to the situation for MnF_2 discussed below. Finally, the magnetic field behavior of the one- and two-magnon lines in FeF_2 is partly illustrated in Fig. 8. The one-magnon excitation $\Delta S^z=\pm1$ splits the line by $\sim$12 cm^{-1} when a field of $\sim$50 kOe is applied to the sample. In contrast, the same field produces no measurable effect on the two-magnon line, indicating that the $|0,+\rangle$ two-magnon state is indeed responsible for the scattering. Figure 8 serves to illustrate that our experiments are sensitive enough to detect an effect were the $|+2,+\rangle$ and/or the $|-2,+\rangle$ states responsible for the second-order scatter-

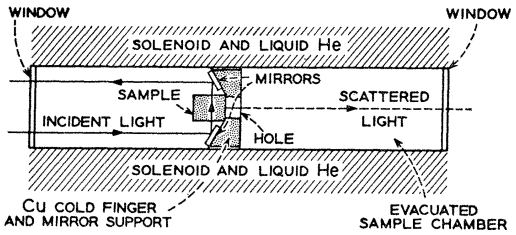

FIG. 5. Schematic of experimental geometry for magnetic field studies. The evacuated sample chamber is 1 in. in diameter by 6 in. long. The Cu insert acts as both a support for the mirrors and the sample and as a cold finger to provide sample cooling.

ing. The magnetic field behavior also eliminates the previously mentioned possibility that the observed scattering might be due to a zone-edge magnon plus a zone-edge phonon, since that excitation carries a spin of 1.

The observations in MnF_2 have so far been limited to the second-order scattering, but the details of line

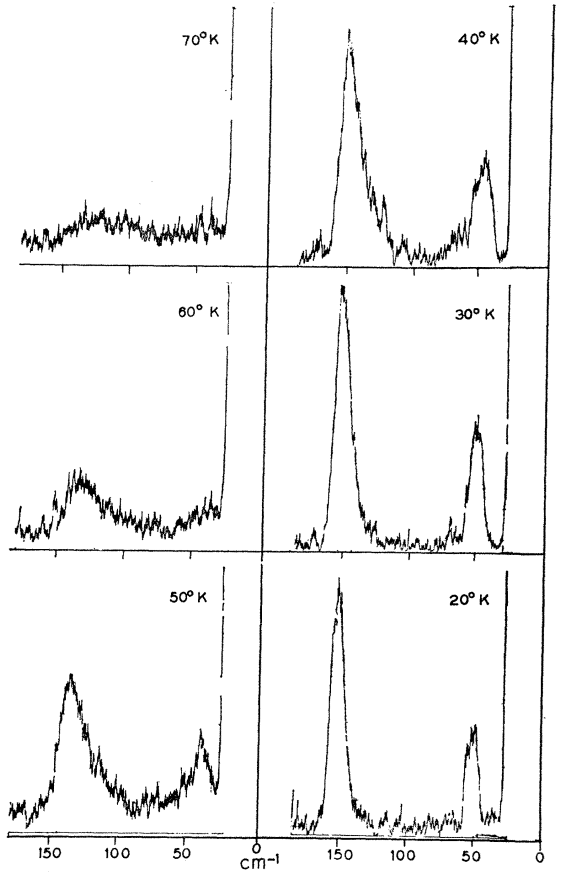

FIG. 6. Stokes scattered light for the XZ geometry at various temperatures in FeF_2. Slit widths necessitated in these early experiments precluded any measure of linewidth or shape for both the one- and two-magnon peaks shown here. Improvement in signal to noise is evident in Fig. 7.

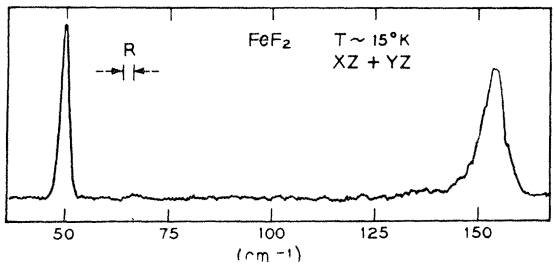

FIG. 7. The magnon spectrum at 15°K in FeF_2. The effective slit width is indicated by R. Here the true line shape of the second-order peak is observed, but the first-order line ($\sim$50 cm^{-1}) is still resolution-limited. The improvement in resolution of course does not alter the ratio of integrated intensities for the first- and second-order scatterings from that in Fig. 6.

shape and the polarization of the scattering are more interesting than in the FeF_2 case. The second-order spectrum in MnF_2 is of about the same intensity as in FeF_2 (corresponding to an extinction coefficient of 10^{-12}–10^{-11} cm^{-1} sr^{-1}). Again the spectrum is unaffected by a strong magnetic field, and the possibility that the scattering is from one phonon plus one magnon is

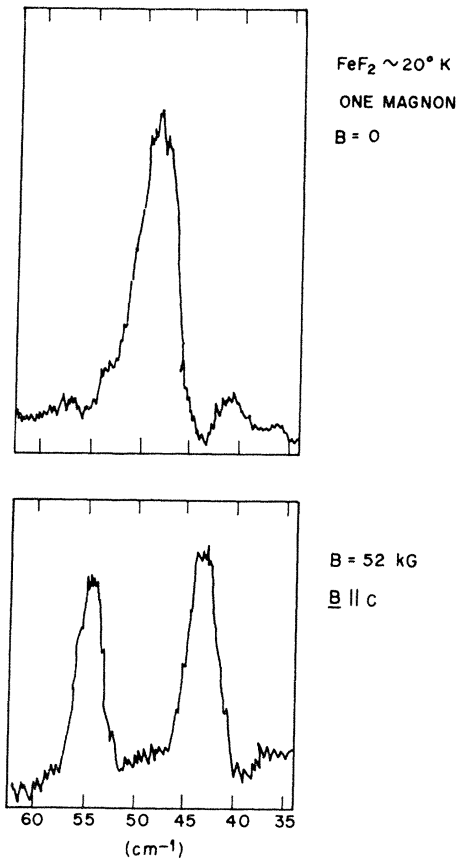

FIG. 8. Splitting of the one-magnon line in FeF_2. (a) No magnetic field applied. (b) $\sim$50 kOe applied $\|$ to c axis. No splitting was observed for $\mathbf{B} \| c$ axis. And no effect could be seen on the two-magnon peak for $\mathbf{B} \perp$ or $\| c$ axis.

eliminated. Again the sharp features of the second-order spectrum appear only in the α_{xz}, α_{yz}, and α_{xy} components. However, as is evident from Fig. 9, the positions and line shapes for the xz and xy components are significantly different, the latter being rather symmetric and centered near 100 cm^{-1}; the former being noticeably asymmetric and cutting off near 110 cm^{-1}. As we will see presently, this effect arises from the different magnon frequencies for different positions on the Brillouin-zone surface.

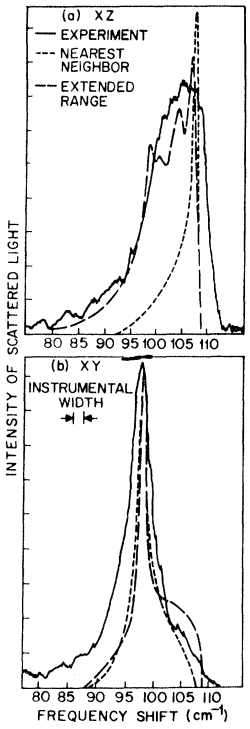

FIG. 9. Theoretical and experimental spectra for two-magnon scattering in MnF_2 at 10°K. Intensity of theoretical curves are normalized to the experimental. (a) XZ experimental geometry; (b) XY geometry. Solid curves are experimental; short dashed curves are theoretical with "nearest-neighbor coupling;" long dashed curves are for "extended range coupling."

We are now in a position to complete the theoretical discussion of the last section and to specialize it to the rutile-structure antiferromagnets.

IV. THEORY FOR MnF_2 AND FeF_2: COMPARISON WITH EXPERIMENT

A. Crystal Structure and Magnons

The crystal structure in the antiferromagnetic phase for MnF_2 and FeF_2 is illustrated in Fig. 10. We rely extensively on the results of and notation used by Dimmock and Wheeler[20] in their discussion of symmetry properties of magnetic crystals. The space group in the antiferromagnetic phase, where the allowed symmetry operations must leave invariant not only the locations of the ions but also their magnetic moments, is D_{2h}^{12} or P_{nnm}.

[20] J. O. Dimmock and R. G. Wheeler, Phys. Rev. **127**, 391 (1962).

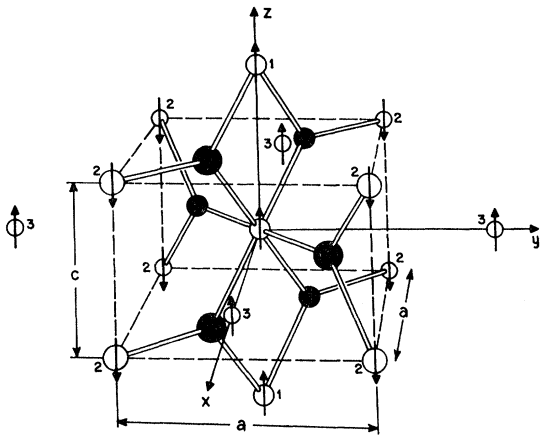

FIG. 10. Unit cell of the magnetic fluoride or rutile structure indicated by the dashed lines. The first, second, and third magnetic neighbors of the central ion are shown. The arrows represent the orientations of the magnetic moments.

The Brillouin zone is illustrated in Fig. 11. The symbols inserted against the symmetry points and symmetry lines indicate the appropriate irreducible representations by which the magnon wave functions $|\uparrow \mathbf{k}\rangle$ and $|\downarrow \mathbf{k}\rangle$ transform. The notation is that of Dimmock and Wheeler,[20] and there is assumed to be no applied external magnetic field. A single symbol in the figure indicates that the pair of magnons is degenerate by group theory at the corresponding sym-

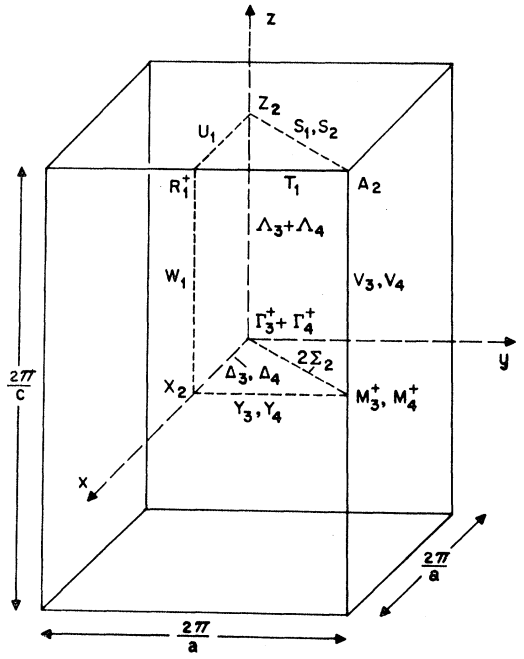

FIG. 11. Brillouin zone of the magnetic fluoride structure showing the symmetry characters of the magnons. The representations at Γ and on the line Λ joined by + signs are degenerate by time-reversal.

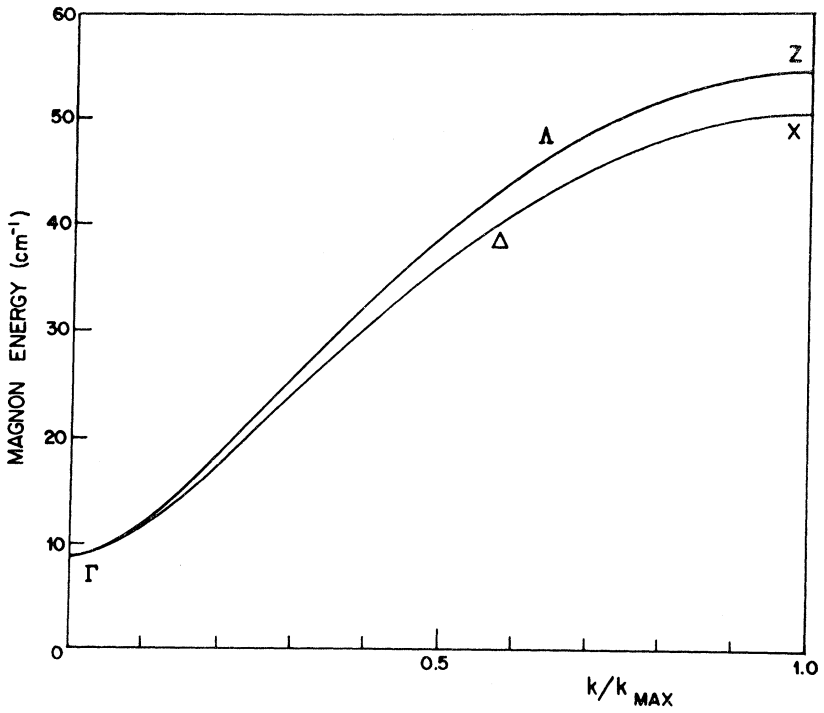

FIG. 12. Magnon dispersion in MnF_2 at 4.2°K in the (100) and (001) directions as determined by neutron scattering in Ref. 21. (Data kindly supplied by Turberfield.)

metry point or line. A pair of symbols indicates that there is no degeneracy, except for the points Γ and Λ where the two one-dimensional representations are degenerate by time-reversal.

Okazaki, Turberfield, and Stevenson[7] have determined the dependence of magnon frequency on wave vector along the lines Λ and Δ in the Brillouin zone for MnF_2 using neutron scattering. Their results are shown in Fig. 12. For both FeF_2 and MnF_2, γ_k given by (7) is determined by a sum over the nearest antiferromagnetically aligned neighbors, which in this case are the second neighbors of a given spin, the nearest neighbors being on the same sublattice. From Fig. 10 the result is seen to be

$$\gamma_k=\cos(\tfrac{1}{2}ak_x)\cos(\tfrac{1}{2}ak_y)\cos(\tfrac{1}{2}ck_z). \quad (46)$$

Thus γ_k is unity at $\mathbf{k}=0$ and decreases uniformly to become zero at all points on the surface of the Brillouin zone. The dispersion relation (16) cited for a simple antiferromagnet predicts ω_k to be independent of $\mathbf{k}$ on the zone surface in contrast to the neutron scattering results and also to our light-scattering results. The dispersion relation may be generalized to include a small ferromagnetic exchange coupling between each spin and its two nearest neighbors and four third neighbors. The result is[7]

$$E_k=\hbar\omega_k=2S\,|\,J_2\,|\,Z_2[(1+\epsilon_k)^2-\gamma_k^2]^{1/2},$$

$$\epsilon_k=(H_A/2SZ_2\,|\,J_2\,|)+(2Z_1J_1/Z_2\,|\,J_2\,|)\sin^2(\tfrac{1}{2}ck_z)$$
$$+(Z_3J_3/Z_2\,|\,J_2\,|)\{\sin^2(\tfrac{1}{2}ak_x)+\sin^2(\tfrac{1}{2}ak_y)\}, \quad (47)$$

where J_1 and J_3 are the exchange interactions along the ⟨001⟩ and ⟨100⟩, ⟨010⟩ directions, respectively, and J_2 is along the ⟨111⟩ direction and replaces J in (16).

The FeF_2 magnons are expected to obey a similar dispersion relation since crystal-field quenching produces a ground-state ion which behaves similarly to a pure spin.

The theoretical dispersion relation predicts the magnons $|\uparrow\mathbf{k}\rangle$ and $|\downarrow\mathbf{k}\rangle$ to be degenerate for all $\mathbf{k}$ in zero applied field. This degeneracy arises[21] because the exchange Hamiltonian has greater symmetry than the lattice. Inclusion of dipolar forces produces a small splitting ($\sim$1 cm^{-1}) of the magnon branches at all points in the zone except where Fig. 11 indicates a degeneracy. No splittings have been detected experimentally.

B. First-Order Scattering

The general features of the first-order scattering from a simple antiferromagnet have been derived in Sec. II C. We now consider the application of this theory to the case of MnF_2-structure antiferromagnets. It is well known[22] that the symmetry of a crystal lattice imposes certain requirements on the symmetry of the light scattering by excitations in the crystal. We here evaluate these symmetry restrictions and relate the results to the more explicit calculations of Sec. II C.

The D_{2h}^{12} space group of MnF_2 in the antiferromagnetic phase increases to D_{4h}^{14} in the paramagnetic

[21] W. Brinkman and R. J. Elliott, J. Appl. Phys. **37**, 1457 (1966); and Proc. Roy. Soc. (London) **A294**, 343 (1966).
[22] R. Loudon, Advan. Phys. **13**, 423 (1964); **14**, 621 (E) (1965).

phase above the Néel temperature[20] where the spin orientations can be ignored and all Mn sites can be treated as equivalent. Below the Néel temperature the space-group operations which occur in D_{4h}^{14} but not in D_{2h}^{12} have the effect of reversing all the spin orientations and are therefore not allowed. They become allowed, however, if they are combined with the operation of time reversal which reinverts the spins to these original directions. Such space-group operations which include time reversal are said to be antiunitary. The operations contained in D_{2h}^{12} do not contain time reversal and are known as the unitary operations. Physical properties of the antiferromagnetic crystal must be invariant under all the space-group operations, both unitary and antiunitary.

It is customary to display the results of a calculation of scattering symmetries in the form of matrices $\alpha_{\sigma\rho}$ defined so that the extinction coefficient is given by

$$h=A\,|\sum_{\rho,\sigma=x,y,z}\epsilon_1^{\sigma}\alpha_{\sigma\rho}\epsilon_2^{\rho}\,|^2, \tag{48}$$

where A is independent of polarization directions. The determination of the matrices $\alpha_{\sigma\rho}$ is a standard group-theoretical exercise, and these matrices have been tabulated for all the nonmagnetic crystal structures.[22]

The α matrices for antiferromagnetic MnF_2 are calculated by exactly the same method as for a nonmagnetic space group, using both the unitary and antiunitary operations of the antiferromagnetic state. There are four types of Raman-active zero-wave-vector excitation having symmetries labeled Γ_1^+, Γ_2^+, Γ_3^+, and Γ_4^+ by Dimmock and Wheeler. The four representations are nondegenerate, but Γ_3^+ and Γ_4^+ are degenerate with each other due to time reversal.[20] As shown in Fig. 11 the magnons in MnF_2 and FeF_2 have symmetry $\Gamma_3^+ + \Gamma_4^+$ at $\mathbf{k}=0$, and we are not interested here in the Γ_1^+ and Γ_2^+ types of excitation. However, such excitations occur in CoF_2 in a frequency region which makes their detection by light scattering experiments feasible.[23]

Table I lists the scattering matrices for all four types of excitation. For the degenerate pair $\Gamma_3^+ + \Gamma_4^+$ the matrices have been chosen so as to refer to the zero-wave-vector magnons $|\downarrow 0\rangle$ and $|\uparrow 0\rangle$. The restrictions imposed by symmetry involve relations between

TABLE I. Raman matrices for antiferromagnetic MnF_2.

$$\begin{bmatrix}\alpha & 0 & 0\\ 0 & \alpha^* & 0\\ 0 & 0 & \beta\end{bmatrix}\quad\begin{bmatrix}0 & 0 & \gamma\\ \gamma^* & 0 & 0\\ 0 & 0 & 0\end{bmatrix}\quad\begin{bmatrix}0 & 0 & \delta\\ 0 & 0 & i\delta^*\\ \epsilon & i\epsilon^* & 0\end{bmatrix}\quad\begin{bmatrix}0 & 0 & -\delta\\ 0 & 0 & i\delta^*\\ -\epsilon & i\epsilon^* & 0\end{bmatrix}$$

$$|\downarrow 0\rangle \qquad |\uparrow 0\rangle$$

$$\Gamma_1^+ \qquad \Gamma_2^+ \qquad \Gamma_3^+ + \Gamma_4^+$$

[23] R. A. Cowley, P. Martel, and R. W. H. Stevenson, Phys. Rev. Letters **18**, 162 (1967).

TABLE II. Symmetry of the two-magnon state $|0,+\rangle$ given by (38) for $\mathbf{k}$ corresponding to Brillouin-zone symmetry points.

Γ	X	M	Z	R	A
Γ_1^+	0	Γ_2^+	0	Γ_3^+ or Γ_4^+	0

complex conjugates of elements of the matrices. This is due to the occurrence of the antiunitary symmetry operations, since time-reversal includes the operation of complex conjugation.

Comparing the $\Gamma_3^+ + \Gamma_4^+$ matrices with the results of the calculation of Sec. II C, it is seen that to obtain agreement between the symmetries of (31) and (48) the additional restrictions $-\epsilon=\delta$ and $\mathrm{Im}\epsilon=\mathrm{Im}\delta=0$ must be imposed on the matrix elements. It is not difficult to see why the calculations leading to (30) and (31) produce a result which is less general than the symmetry of the lattice would allow. In the first place the magnetic ions were assumed to have S-type ground states appropriate to Mn^{2+} and the orbitally quenched ground state of Fe^{2+}. As discussed after (27) relaxation of this condition leads to a scattering matrix which is not purely antisymmetric in the components of $\mathbf{E}_1$ and $\mathbf{E}_2$. Such lack of antisymmetry may be observable in CoF_2, where the ground-state orbital momentum is not quenched, but for FeF_2 the antisymmetry condition $-\epsilon=\delta$ is well satisfied experimentally (see Sec. III).

The second lack of generality in (31) is due to treating the ions on the two sublattices as having identical wave functions and energy levels. It is seen in Fig. 10 that the symmetries of the fluorine configurations about the two types of site differ by a 90° rotation. This leads to differences in the orthorhombic crystal-field components of the ionic wave functions and ultimately to imaginary components in the matrix elements ϵ and δ. For Mn^{2+}, which has a true S ground state, the orthorhombic splittings of the odd-parity excited states are very small compared to the excitation energy of these states and it is a good approximation to treat the two types of ionic state as equivalent. The same approximation may be valid in Fe^{2+}, although Moriya[24] has argued that the lack of equivalence between the two sites in FeF_2 may lead to significant imaginary components in ϵ and δ. Such components lead to an extinction coefficient similar to (31) but having $(u_0+v_0)^2$ replaced by $(u_0-v_0)^2$. This produces a small change in the magnitude of h for FeF_2. The observed value of h for FeF_2 given in Sec. III in fact lies slightly below the lower end of the predicted range given by (27) with the additional antiferromagnetic factor included.

As mentioned above, the magnon frequency and its temperature dependence agree with previous results of antiferromagnetic resonance experiments. The split-

[24] T. Moriya (private communication); J. Appl. Phys. **39**, 1042 (1968).

ting of the first-order line in a magnetic field is $4\beta H_0$, in agreement with (18) for $g=2$.

C. Second-Order Scattering

We have already presented experimental evidence that the second-order scattering in both MnF_2 and FeF_2 is due to the $|0,+\rangle$ two-magnon states. We now use this fact to derive additional predictions for the D_{2h}^{12} materials. The density-of-states curve for the magnons has sharp critical-point discontinuities of slope at the magnon frequencies for the symmetry points Γ, X, M, Z, R, and A in the Brillouin zone (see Ref. 15 for a calculation of the magnon density of states in MnF_2). The slope discontinuity corresponding to a particular symmetry point should also appear as a feature in the second-order Raman spectrum provided that the scattering is an allowed process for the $|0,+\rangle$ pair of magnons at the given symmetry point.

Table II shows the symmetry of $|0,+\rangle$ corresponding to the symmetry points. A zero entry indicates that $|0,+\rangle$ vanishes at the corresponding symmetry point. For point R, the state $|0,+\rangle$ has a symmetry which is different for the two examples of this type of point which occur in the Brillouin zone (see Fig. 11). Comparing Tables I and II, it is seen that the critical point Γ contributes to the second-order scattering for polarization components xx, yy, and zz (here xx is shorthand for $E_1^xE_2^x$, etc.); M contributes for xy and yx; and R contributes for xz, zx, yz, and zy.

To obtain more information on the second-order spectrum and its relation to the symmetry of the magnons in the Brillouin zone we set up a spin Hamiltonian for the two-magnon process.

We must sum the matrix element M_{ij} given by (44) or (45) over all pairs of ions i and j on the opposite sublattices, taking account of the requirements imposed by the symmetry of the D_{2h}^{12} lattice. Since the matrix element includes an exchange integral between the pair of ions, M_{ij} will diminish with increasing separation of the ions. As a first approximation we restrict the summation to nearest neighbors on opposite sublattices. The simplest procedure is to determine the most general form of spin Hamiltonian which is proportional to a component of $\mathbf{E}_1$, a component of $\mathbf{E}_2$, and to the spin combinations $S_i^+S_j^-$ and $S_i^-S_j^+$. Crystal symmetry requires the resulting Hamiltonian H_S to be invariant under all the operations of the antiferromagnetic space group, i.e., H_S must transform like Γ_1^+.

As shown by (40) the operator $S_i^xS_j^x+S_i^yS_j^y$ is the type required to excite the two-magnon state $|0,+\rangle$. This spin function transforms like Γ_1^+ in the antiferromagnetic group. In forming the spin Hamiltonian the relative phases of the contributions of the eight neighbors i of a given spin i can be adjusted by introducing a vector $\boldsymbol{\sigma}^{ij}$ defined by

$$\sigma_{ij}{}^{\alpha}=\text{sign}(\mathbf{r}_j-\mathbf{r}_i)_\alpha, \qquad \alpha=x,y,z, \tag{49}$$

where $\mathbf{r}_j-\mathbf{r}_i$ is the vector connecting ions i and j. Thus the $\sigma_{ij}{}^{\alpha}$ are equal to either $+1$ or -1 and merely determine the relative signs of terms in the i,j summation.

To form H_S we multiply the spin operator by those combinations of $\mathbf{E}_1$, $\mathbf{E}_2$, and $\boldsymbol{\sigma}^{ij}$ which belong to Γ_1^+. This ensures that H_S transforms like Γ_1^+. The required combinations are

$$E_1{}^zE_2{}^z; \qquad (E_1{}^xE_2{}^x+E_1{}^yE_2{}^y);$$

$$(E_1{}^xE_2{}^y+E_1{}^yE_2{}^x)\sigma_x{}^{ij}\sigma_y{}^{ij};$$

$$(E_1{}^xE_2{}^z+E_1{}^zE_2{}^x)\sigma_x{}^{ij}\sigma_z{}^{ij}+(E_1{}^yE_2{}^z+E_1{}^zE_2{}^y)\sigma_y{}^{ij}\sigma_z{}^{ij};$$

and

$$(E_1{}^xE_2{}^z-E_1{}^zE_2{}^x)\sigma_x{}^{ij}\sigma_z{}^{ij}+(E_1{}^yE_2{}^z-E_1{}^zE_2{}^y)\sigma_y{}^{ij}\sigma_z{}^{ij}. \tag{50}$$

From these considerations then the required spin Hamiltonian is

$$\begin{aligned}H_S=\sum_{\langle i,j\rangle}\{&A(E_1{}^xE_2{}^x+E_1{}^yE_2{}^y)+BE_1{}^zE_2{}^z\\&+C(E_1{}^xE_2{}^y+E_1{}^yE_2{}^x)\sigma_x{}^{ij}\sigma_y{}^{ij}+D[(E_1{}^yE_2{}^z+E_1{}^zE_2{}^y)\sigma_y{}^{ij}\sigma_z{}^{ij}\\&+(E_1{}^xE_2{}^z+E_1{}^zE_2{}^x)\sigma_x{}^{ij}\sigma_z{}^{ij}]+F[(E_1{}^yE_2{}^z-E_1{}^zE_2{}^y)\sigma_y{}^{ij}\sigma_z{}^{ij}\\&-(E_1{}^zE_2{}^x-E_1{}^xE_2{}^z)\sigma_x{}^{ij}\sigma_z{}^{ij}]\}(S_i{}^xS_j{}^x+S_i{}^yS_j{}^y).\end{aligned} \tag{51}$$

In this expression A, B, C, D, and F are coupling constants determined by (44) with the electric fields and spin operators removed and appropriate components of $\mathbf{r}_1$ and $\mathbf{r}_2$ substituted. Since experiment (see Sec. III) shows the second-order scattering to be symmetric we conclude that F is negligible for MnF_2 and FeF_2 even though the presence of this term is allowed by symmetry. There is a close analogy between (51) and the spin Hamiltonian which controls the two-magnon electric-dipole absorption process.[15]

The summations over spin operators in (51) can be replaced by summations over magnon operators by use of (10). We consider as an example the part of the spin Hamiltonian in the product of the x and y components of the fields. The xy Stokes-scattering extinction coefficient per unit frequency interval of scattered radiation is

$$\begin{aligned}h^{xy}(\omega_2)=&(64S^2\eta_2\omega_1\omega_2{}^3C^2/V\eta_1c^4)(\epsilon_1{}^x\epsilon_2{}^y+\epsilon_1{}^y\epsilon_2{}^x)^2\\&\times\sum_{\mathbf{k}}(n_{\mathbf{k}}+1)^2(u_{\mathbf{k}}{}^2+v_{\mathbf{k}}{}^2)^2\sin^2(\tfrac{1}{2}ak_z)\sin^2(\tfrac{1}{2}ak_y)\\&\times\cos^2(\tfrac{1}{2}ck_z)\delta(\omega_1-\omega_2-2\omega_{\mathbf{k}}).\end{aligned} \tag{52}$$

Other polarizations give quite similar expressions but with different trigonometric terms. These trigonometric factors provide the weightings of the magnon density of states which emphasize particular regions in the Brillouin zone and thus determine the shape of the second-order spectrum. In Table III we list the bilinear electric field components, their corresponding trigonometric factors, and the critical points they emphasize.

Note that the latter agree with the results derived earlier in the present subsection.

The spectra calculated using (52) for h^{xy} and a similar expression for h^{xz} are compared to the experimental results for MnF_2 in Fig. 9. The anisotropy field and first-, second-, and third-neighbor exchange constants used here are $H_A=1.05°K$, $J_1=0.35°K$, $J_2=-1.735°K$, and $J_3=-0.025°K$ and are consistent with the neutron scattering data of Okazaki *et al.*[7] Even for this "nearest-neighbor" approximation (indicated by the short dashed curves) the gross features of the spectra—position and symmetric versus asymmetric shape—are correctly predicted. The xz spectrum lies at approximately $2\omega_R$ while the xy lies at $2\omega_M$. The theoretical spectrum for the xx, yy, and zz polarizations is broad, flat, and featureless in agreement with the lack of any detectable scattering for these polarizations.

Agreement with experiment is greatly improved by lifting the restriction on the sum over M_{ij} to nearest neighbors and assuming a more realistic falloff to include more distant neighbors. The long dashed curves in Fig. 9 result from assuming an exponential falloff $\exp[(-|\mathbf{r}_j-\mathbf{r}_i|)/r_0]$ with $r_0=0.4a$, and a is the lattice constant. The same procedure was followed with success in the case of two-magnon electric-dipole absorption in MnF_2.[15]

In view of the success of the excited-state exchange mechanism in explaining the MnF_2 results, it is unlikely that the phonon modulation of the ground-state exchange matrix elements, which was mentioned above as a possible scattering mechanism, is of any importance here. Since the phonon-modulation theory relies on the ordinary ground-state exchange integrals, the range of the scattering interaction would be expected to be the same as the range of the exchange integrals themselves. The longer range of interaction required to explain the experiments can be accounted for in the excited-state exchange theory in terms of the odd-parity excited-state wave functions being more extended in space than the ground-state wave functions which determine the ordinary exchange integrals.

It is evident from the form of the dispersion relation (47) that the anisotropy of the magnon energy of the Brillouin-zone surface is due to J_1 and J_3. That J_1 is appreciable for MnF_2 is seen from the difference in peak frequencies of the xy and xz spectra. The high-frequency cutoff in the xz spectrum should give the highest magnon frequency in the Brillouin zone. The second-order spectrum thus contains a good deal of information about magnons at extremal regions of the Brillouin zone. Indeed, were the zone-center magnon frequency available from first-order scattering in MnF_2, this together with the above analysis of the second-order spectrum and (47) would provide a rather complete picture of the entire magnon dispersion relation.

In fact we may follow just such a procedure in FeF_2. From the first-order scattering we know the Γ-point magnon frequency to be 53 cm^{-1}. From the second-order scattering we know the zone-edge frequency to be 154 cm^{-1}. The fact that the second-order xz and xy spectra for FeF_2 are at the same frequency implies that J_1 and J_3 are negligible in this material. The magnon dispersion relation in FeF_2 can be adequately described by (47) with the values $H_A=29.9°K$, $J_2=-2.52°K$, $J_3=J_1\approx 0$; all determined from the light-scattering experiments.

The single remaining experimental quantity to be compared with theory is the ratio of integrated intensities for the first-order scattering (spin-orbit mechanism) and the second-order scattering (exchange mechanism).

The main features in the second-order spectra are caused by magnons close to the zone boundary for which $u_k\approx 1$ and $v_k\approx 0$. Assuming also a sufficiently low temperature that n_k can be neglected, (52) can be integrated to give the total scattering:

$$h_2=\int h_2(\omega_2)\,d\omega_2$$
$$=(8SM_s\eta_2\omega_1\omega_2C^2/g\beta\eta_1c^4)\,(\epsilon_1{}^x\epsilon_2{}^y+\epsilon_1{}^y\epsilon_2{}^x). \quad (53)$$

It is interesting to compare this with the result (31) for first-order scattering. Denoting the order of the scattering by subscripts on h,

$$(h_2/h_1)\simeq[4SC^2/(u_0+v_0)^2\Gamma^2], \quad (54)$$

assuming that the polarization factors are both unity.

To get a rough estimate for the size of this ratio we use the approximations (24) and (45) for Γ and C, respectively, assuming the $\mathbf{r}$ matrix elements to be equal and taking the limit $E_0\gg\hbar\omega_1$ and $\hbar\omega_2$. This leads to the very rough estimate

$$(h_2/h_1)\approx[4S/(u_0+v_0)^2](32V^2E_0{}^2/\lambda^2\hbar^2\omega_1{}^2). \quad (55)$$

For MnF_2, taking $E_0\approx 5\hbar\omega_1$, and $\lambda\approx 1000$ cm^{-1} (we are indebted to A. Kiel for this estimate), the above ratio is about $V^2/10$, where V is in cm^{-1}. A similar estimate for FeF_2 gives $V^2/60$. The experimental ratio for the latter crystal is about 2–3, suggesting $V\approx 10$ cm^{-1}, which is the same value as found by Tanabe *et al.*,[16] for the somewhat similar exchange matrix element which controls the two-magnon absorption in FeF_2. If

TABLE III. Electric-field polarizations with corresponding weighting factors and emphasized critical points.

$E_1{}^xE_2{}^x$; $E_1{}^yE_2{}^y$; $E_1{}^zE_2{}^z$	$\cdots\cos(\frac{1}{2}ak_x)\cos(\frac{1}{2}ak_y)\cos(\frac{1}{2}ck_z)\cdots\Gamma$
$E_1{}^xE_2{}^y$; $E_1{}^yE_2{}^x$	$\cdots\sin(\frac{1}{2}ak_x)\sin(\frac{1}{2}ak_y)\cos(\frac{1}{2}ck_z)\cdots M$
$E_1{}^xE_2{}^z$; $E_1{}^zE_2{}^x$	$\cdots\sin(\frac{1}{2}ak_x)\cos(\frac{1}{2}ak_y)\sin(\frac{1}{2}ck_z)\cdots R$
$E_1{}^yE_2{}^z$; $E_1{}^zE_2{}^y$	$\cdots\cos(\frac{1}{2}ak_x)\sin(\frac{1}{2}ak_y)\sin(\frac{1}{2}ck_z)\cdots R$

V is the same for MnF_2 then (55) predicts the intensity of the first-order line to be only $\frac{1}{10}$ that of the second-order peak.

V. CONCLUSION

To the methods for studying spin waves—neutron scattering, infrared absorption, optical sideband absorption—has been added another: inelastic light scattering. In the above paper we have presented the theory for both one- and two-magnon light scattering and have explained our experimental results in MnF_2 and FeF_2. It was shown that details of the magnon dispersion relation could be extracted from the spectra of scattered light. We should note that for the D_{2h}^{12} materials the selection rules for two-magnon scattering, two-magnon absorption, and optical-magnon sidebands are all different—so the experimental methods are complementary. We should also note that the ability to study magnons at the zone center and the zone edge in the same experiment is best suited to light scattering. In at least one case—NiF_2—studies of zone-edge magnons by two-magnon absorption are not possible due to a strong infrared-active phonon (E_u) at $\sim$225 cm^{-1}. However, since this phonon is not Raman active, it has not interfered with the study of the zone-edge magnon by second-order light scattering.[6]

All of the magnetic materials thus far examined by light scattering have quite simple magnon branches. But as techniques improve and experience grows it is quite likely that the use of light scattering will become much more important in the study of magnetic materials.

ACKNOWLEDGMENTS

We are grateful to J. P. Hurrell and S. P. S. Porto for helpful comments and suggestions and to C. A. Lambert for computer assistance. We also thank H. J. Guggenheim for the excellent samples of MnF_2 and FeF_2, H. L. Carter and D. H. Olson for technical assistance, A. Albert for crystal polishing and M. B. Graifman for advice on the temperature control system. We are indebted to Professor T. Moriya for a report of his theory of magnon scattering prior to publication.

PHYSICAL REVIEW VOLUME 166, NUMBER 2 10 FEBRUARY 1968

Spin-Lattice Interaction in UO_2. I. Ground-State and Spin-Wave Excitations

S. J. Allen, Jr.
Bell Telephone Laboratories, Murray Hill, New Jersey
(Received 8 August 1967)

A microscopic theory of the effect of spin-lattice interaction on the ground-state and spin-wave excitations in UO_2 is presented. Three parameters required by a Jahn-Teller description of the local spin-lattice interactions and an exchange constant are introduced as basic variables to describe the system at $T=0°K$. The spin-lattice ground state reveals a competition between the Jahn-Teller forces and the exchange energy that results in a reduction of the magnitude of the spin. It is also shown that the indirect quadrupole-quadrupole interaction caused by the virtual exchange of an optical phonon is as large as the exchange coupling ($\sim$30°K), and significantly modifies the spin-wave energies and wave functions. Values for the interaction parameters are obtained by fitting the theory to the excitation spectra and to wave functions deduced from far-infrared absorption spectroscopy and from the inelastic scattering of neutrons. The theory is consistent with the upper limits placed on the lattice distortion and with the anomolous behavior of the elastic constant C_{44}.

I. INTRODUCTION

THE ground-state degeneracy of a concentrated system of magnetic ions at $T=0°K$ is usually lifted by the exchange interaction. However, if the single-ion ground state is orbitally degenerate and possesses an even number of electrons, interesting alternatives to the exchange splitting may occur. These usually manifest themselves as electrostatic quadrupole-quadrupole interactions or cooperative Jahn-Teller distortions. The electrostatic interactions appear to be comparable with the exchange interaction in the rare-earth[1] and probably the actinide-series insulators. Uranium dioxide appears to be a particularly striking example of this situation. The ground-state degeneracy is largely due to the unquenched orbital motion of the two $5f$ electrons and there is evidence that the interaction between the spin and the lattice is as strong as the exchange interaction between pairs.[2,3]

In the present paper a microscopic theory of the ground electronic state and elementary electronic excitations (spin waves) is described. The basic interaction between the local spin and the distortion of the nearby lattice is parametrized by a set of constants prescribed

[1] R. J. Birgeneau, M. T. Hutchings, and R. N. Rogers, Phys. Rev. Letters **16**, 584 (1966); R. Finkelstein and A. Mencher, J. Chem. Phys. **21**, 472 (1952); B. Bleaney, Proc. Phys. Soc. (London) **77**, 113 (1961); J. M. Baker and A. F. Mau, Can. J. Phys. **45**, 403 (1967).

[2] G. Dolling and R. A. Cowley, Phys. Rev. Letters **16**, 683 (1966).

[3] O. G. Brandt and C. T. Walker, Phys. Rev. Letters **18**, 11 (1967).